Journal of the Optical Society of America B
OPTICAL PHYSICS

Impact of delayed feedback of arbitrary duration in self-pulsations of a CO_2 laser

LEANDRO JUNGES[1,2] AND JASON A. C. GALLAS[1,2,3,*]

[1]Departamento de Física, Universidade Federal da Paraíba 58051-970 João Pessoa, Brazil
[2]Instituto de Altos Estudos da Paraíba, Rua Infante Dom Henrique 100-1801 58039-150 João Pessoa, Brazil
[3]Institute for Multiscale Simulations, Friedrich-Alexander Universität Erlangen-Nürnberg, D-91052 Erlangen, Germany
*Corresponding author: jason.gallas@cbi.uni-erlangen.de

Received 18 November 2015; revised 12 January 2016; accepted 12 January 2016; posted 14 January 2016 (Doc. ID 254082); published 18 February 2016

We report on a systematic investigation of the stability of a CO_2 laser subjected to delayed electro-optical feedback. Such a laser roughly displays three operational intervals of stability, which we characterize using high-resolution stability charts and a video. Contrary to current belief, we find delays smaller than ∼1 μs to strongly "clean complexity," namely, to prevent chaos and periodic pulsations with many spikes. In contrast, complex pulsations and chaos are significantly enhanced for $\tau > 1$ μs. In this range, one finds a complex alternation of periodic and chaotic phases, which are sensitive to the delay duration.

OCIS codes: (140.3470) Lasers, carbon dioxide; (190.0190) Nonlinear optics; (190.3100) Instabilities and chaos.

http://dx.doi.org/10.1364/JOSAB.33.000373

1. INTRODUCTION

The study of the distribution of self-pulsations generated by lasers with feedback is attracting increasing attention [1–10]. In CO_2 lasers, feedback is known to induce rich dynamics such as period-doubling cascades, Shilnikov homoclinic chaos, intermittency, multistability, delayed bifurcation, quasi-periodicity, and more [11–29]. In particular, the first quantum optics device to experimentally reveal the presence of deterministic chaos and multistability was a Q-switched CO_2 laser operating with modulated parameters [25–27].

The CO_2 laser is a class B laser [28] described by two rate equations for the laser intensity and population inversion. But class B lasers display no irregular spiking because the Poincaré–Bendixson theorem forbids them in dimensions smaller than three [24,29]. A popular method to bypass this restriction is by implementing a feedback loop that adds an extra degree of freedom and allows complex bursting and spiking [4–10]. A common feedback mechanism involves tuning the feedback gain [10,14,21]. Extending an interesting work by Yang *et al.* [21], we reported stability diagrams revealing a plethora of unanticipated regularities such as frequency and peak discontinuities in the control space, and pattern complexification based on certain *pulse deformations* [7]. However, our previous work considered only the case of *instantaneous* feedback.

A considerably more realistic situation involves considering the impact of a *time-delayed* feedback loop. In this case, several distinct periodic regimes, characterized by different amplitude and frequency, may be possible for identical or nearly identical values of the control parameters [22,23]. Such abundance of regimes is usually difficult to quantify exhaustively [29–31]. Furthermore, delayed feedback implies the creation of an infinite number of degrees of freedom. This brutal increase of the phase-space dimensionality makes the analysis of lasers with delay a challenging task, which has been much less addressed thus far. However, lasers with delayed feedback have important practical applications, especially in the context of chaos control (see, e.g., [32,33] and references therein).

The aim of the present paper is to report a systematic numerical study of the impact of a feedback delay-time τ of arbitrary duration on self-pulsations of a CO_2 laser. For three distinct control parameter planes, we provide high-resolution stability charts and a video illustrating how the stability phases evolve when parameters are tuned over extended intervals. Such phases correspond to distinct self-pulsation modes of the laser and are investigated for delays $0 \leq \tau \leq 30$ μs. We find that this interval of τ can be roughly subdivided into three classes of stability behavior, as illustrated by the video in the accompanying supplementary material. Before discussing these classes and the novelties underlying them, we first describe how they are obtained and their main characteristics.

2. CO_2 LASER WITH DELAYED FEEDBACK

The laser considered involves three variables: $x(t)$, the laser intensity normalized to the saturation value, $y(t)$, the population inversion normalized to the threshold value, and $z(t)$, the feedback voltage normalized to $1/\pi$ times the voltage

of the electro-optic modulator. It is governed by the equations [34]

$$\dot{x} = kx(y - 1 - \alpha \sin^2(z(t - \tau)), \quad (1)$$

$$\dot{y} = \gamma(A - y - xy), \quad (2)$$

$$\dot{z} = \beta(B - rx - z), \quad (3)$$

where τ represents feedback delay. Here, k stands for the unmodulated cavity loss, γ for the population decay rate, β for the damping rate of the feedback loop, r is the feedback gain, B is the bias voltage applied to an electro-optic modulator, A is the normalized pump parameter, and α is the amplitude of the modulation [18]. As usual [11–18], B is normalized to $1/\pi$ times the half-wavelength voltage of the modulator. Following the literature, we fix $A = 1.66$, $\alpha = 5.8$, $k = 9.6 \times 10^6$ s^{-1}, $\gamma = 0.03 \times 10^6$ s^{-1}, and $\beta = 0.5 \times 10^6$ s^{-1}. Our goal is to investigate how the stability phases change with τ in the $r \times B$ control plane. As mentioned, for $\tau = 0$ μs (no time delay), the dynamics were revisited and extended by us [7], where an in-depth study of laser phases in the $r \times B$ control parameter plane was presented. Such $\tau = 0$ μs stability diagrams serve as reference to contrast the changes induced by delays of arbitrary duration.

Laser self-pulsations were obtained by solving Eqs. (1)–(3) numerically in a similar way as described elsewhere [35], namely, over a grid of equally spaced points, using the standard fourth-order Runge–Kutta algorithm with a fixed time-step of the order of 10^{-3}. A transient of 10^7 steps was discarded with the subsequent 10^6 steps considered as the asymptotic solution. Integrations were always started from a fixed initial condition, $x(0) = y(0) = 1$, and from the same initial history $z(-\tau, 0) = 1$. The computation of high-resolution diagrams is a quite demanding task that we performed on 1536 high-performance processors of a SGI Altix cluster having a theoretical peak performance of 16 Tflops. For each solution, we counted the number of peaks of $x(t)$, determining from them whether or not the pulses repeated.

Similarly to what happens for ordinary differential equations, the choice of initial configuration is also important when dealing with delayed systems, specially when multistability is involved (see [36]). The infinite number of initial conditions and initial histories precludes a systematic exploration of their effect. For this reason, in this work we opted to work with the aforementioned fixed initial conditions. However, we performed some *ad hoc* tests, which seem to indicate that our results are robust when replacing the above constants by other ones. A detailed investigation of initial conditions and history is a too demanding task, beyond the scope of this work. It is left as an open problem.

Figure 1 illustrates typical examples of the results obtained. Some panels are representative snapshots extracted from the accompanying video. Colors denote the number of spikes per period of the oscillations while lack of numerically detectable periodicity is interpreted as "chaos" and plotted in black. The number of spikes is recorded using 17 colors chosen arbitrarily and organized so as to maximize contrast at the transition boundaries of the several phases. Patterns with more than 17 spikes were plotted "recycling colors mod 17," i.e., by taking as their color index the remainder of the integer division of the number of peaks by 17. Fixed points (i.e., nonoscillatory laser intensity) were plotted using two additional colors: orange for constant nonzero laser intensity, and white for no-lasing ($x = 0$) solutions. For details, see [37–43].

Note that representing laser oscillations in terms of the so-called isospike diagrams [37–43] shown in Fig. 1, i.e., recording the number of spikes per period provides a much more informative representation than the familiar diagrams in terms of Lyapunov exponents [44]. Isospike diagrams are not only able to discriminate periodicity from chaos (as Lyapunov exponents do) but, in addition, illustrate simultaneously how laser pulsations sharing a common waveform (i.e., the same number of spikes per pulse) organize themselves [43,44].

3. IMPACT OF THE DELAYED FEEDBACK

The sizable changes undergone by the laser stability in the $r \times B$ control plane may be seen in Fig. 1. As mentioned, this figure presents a selection of snapshots for $\tau = 0$ up to $\tau = 30$, in units of 10^{-6} s, the first few taken from the video. For $\tau = 0$ μs (no delay), the leftmost panel on the top row in Fig. 1 coincides with results from the literature [7], as expected. The other panels illustrate what happens as τ grows.

First stability range. Initially, when increasing τ from $\tau = 0$ to about $\tau = 0.55$ μs, there is a strong reduction of all complex oscillations. As illustrated in Fig. 1 and detailed in the video, all phases corresponding to oscillations having more than one peak per period shrink quite rapidly. This phase reduction persists up to about $\tau = 0.55$ μs, despite the infinite increase of the dimensionality of the phase space. Thus, in sharp contrast with popular folklore, the initial impact of the delay is to wash out all complex oscillations from the laser.

Second stability range. From $\tau \approx 0.55$ μs up to about $\tau \approx 1.1$ μs, Fig. 1 and the video show that only a large phase of pulsations with one spike per period survives. To the best of our knowledge, this unexpected constant behavior was not previously anticipated, neither by simulations nor by approximate calculations. Because this stability range has a rather large magnitude, it should be possible to detect it in experiments.

Third stability range. Finally, for $\tau \gtrsim 1.1$ μs the complex phases start to reemerge, the first being a green phase associated to solutions with two spikes per period (see Visualization 1). Further increase of the delay time makes this two-peaks region to grow steadily. Additionally, some complicated arrangements of islands of solutions having distinct numbers of peaks start to develop "inside" the green phase. Some of these islands may be seen in Fig. 1, inside the boxes in the panels for $\tau = 3.0$ μs and $\tau = 3.5$ μs. As τ grows such islands also grow, with additional islands proliferating inside them, revealing a nested series of peak-doubling and peak-adding cascades that lead to a region of chaotic solutions inside these concentric islands. As the video shows, increasing the delay beyond about $\tau = 4$ μs, the regions of complex and chaotic solutions grow and an accumulation of the so-called *shrimps* [45–47] can be observed to develop inside them. At this stage, the dynamics are complex and rich. The snapshots for $\tau = 15$ μs and $\tau = 30$ μs illustrate the situations typically observed for large τ.

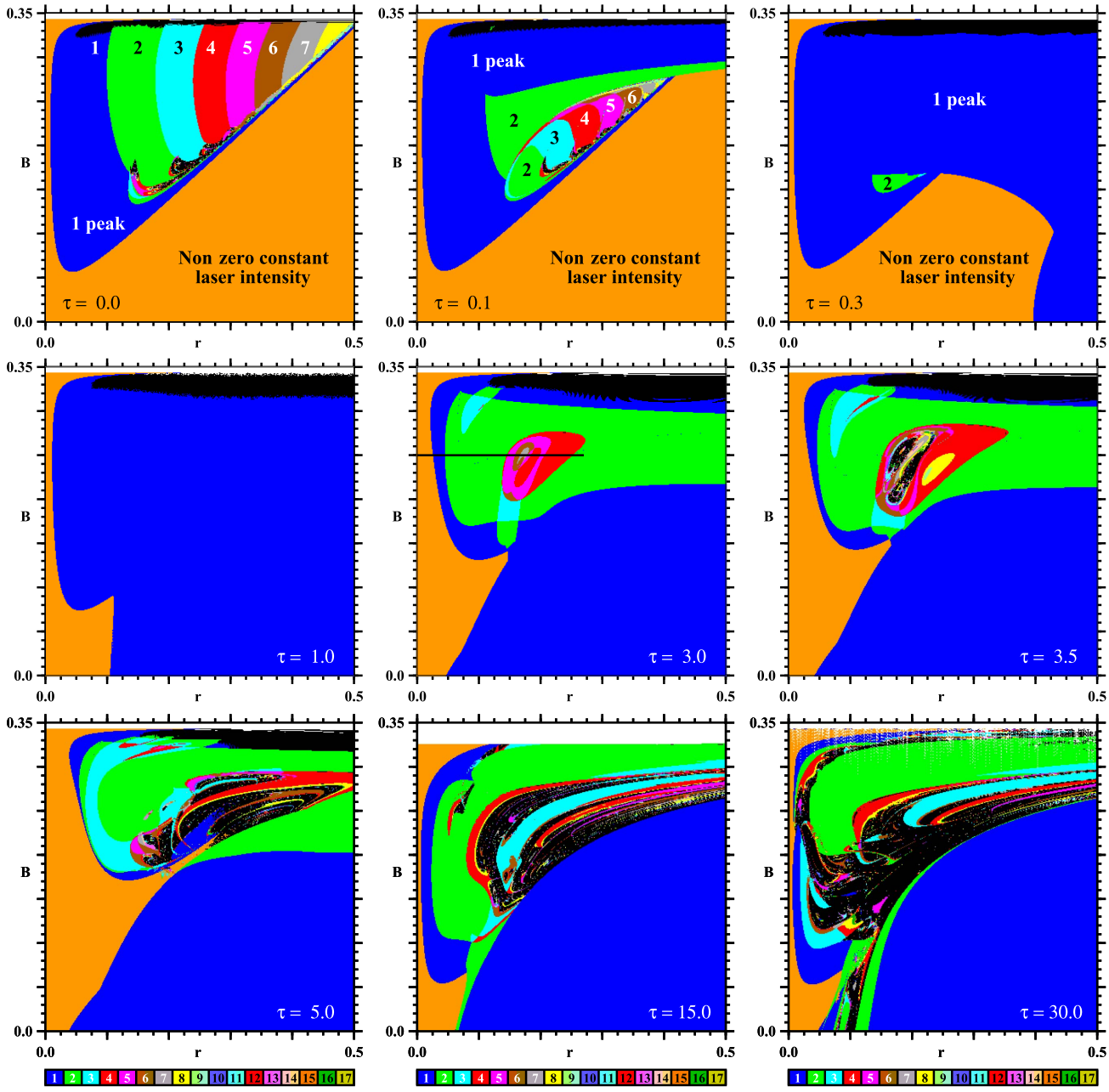

Fig. 1. Illustrative snapshots from the video in the supplementary material, displaying the evolution of representative laser stability diagram when the delay τ, in μs, increases. For $\tau = 0$ μs, pulses in adjacent windows differ by one spike, configuring the presence of a horizontal spike adding cascading of pulses. Initially, the effect of chaos is to reduce complex oscillations; then comes an interval $0.55 \gtrsim \tau \gtrsim 1.1$ μs where a large phase of 1-peak oscillations dominates. For $\tau > 1.1$ μs the complex phases emerge again, with rather intricate distributions of pulses (see text and the video). The panel for $\tau = 3$ μs shows a horizontal line for $0 < r < 0.27$ at $B = 0.25$. A bifurcation diagram along this line is discussed in Fig. 2. Each panel depicts full phase-space analysis performed for $400 \times 400 = 1.6 \times 10^5$ parameter points. The video is a sequence of 200 similar panels (Visualization 1).

The narrow white horizontal stripes on the top of the diagrams in Fig. 1 represent parameter values for which the laser output is identically zero. Below the white stripes, there is a narrow phase in black representing solutions with periods too big to be ascertained without much numerical effort. For a detailed description of the divergence of the period in this specific region, see [7,21].

An important point to stress here is the relative *invariance* of the large one-spike laser phase observed for $0.5 \lesssim \tau \lesssim 1.1$ μs and that separates two regimes where complex dynamical activity is observed. The differences observed in the qualitative behavior before and after this rather bulky invariant interval of τ emphasize the importance of the numerical calculation presented here. Most analytical calculations done in the context of delayed-differential equations are interesting and laborious approximations derived for two opposite limits: either for small or very big delays, mainly for semiconductor lasers [10,48–52] (not for the CO_2 laser discussed in the present paper).

Furthermore, the approximate analytical methods in existence focus on the stability analysis of constant or simple periodic solutions. Such methods are inadequate to extract insight about the complex oscillations addressed in the present paper, which involve a continuous spectrum of delay times and oscillations of arbitrary periods and waveforms.

A criterion for the short-delay regime was postulated by Arecchi *et al.* [34] to be $\tau \lesssim 1/\beta$. For $\beta = 0.5 \times 10^6$ s^{-1}, their definition implies short delays to be delimited by $\tau \lesssim 2$ μs. We have been unable to compare our results with theirs because the experimental data omits needed parameters while model parameters seem to contain inconsistencies.

The video in the supplementary material is an animation of 200 equally spaced snapshots showing how the $r \times B$ laser phases evolve as a function of $\tau \in [0, 10]$ μs. Each snapshot shows $400 \times 400 = 1.6 \times 10^5$ pixels, summarizing results for a total of 32×10^6 parameters, a subset of a much larger number of parameters that were investigated. Using, say, 50 processors simultaneously, it takes about 3.8 h to generate a single frame. On a single processor, the total time required to produce the video would be $200 \times 50 \times 3.8 = 38.000$ h, i.e., about 1580 days or, equivalently, 4.3 years.

The mechanism underlying the creation of shrimps is manifested in the video: the islands that emerge embedded in the chaotic phases are continuously reshaped with the growth of the delay time, resulting in a distribution of nested shrimps. In other words, the emergent islands of new stable laser modes are responsible for the genesis of the shrimps in parameter space. Such details would not be possible to observe without the smooth variation of τ in the video.

4. BIFURCATIONS BY DEFORMATION

As described in the previous section, an increase of the delay τ tends to change the diagrams of Fig. 1 such that some islands of periodic solutions emerge within wide regions associated to solutions with a specific number of peaks or inside regions of nonperiodic behavior. The dynamical features observed for

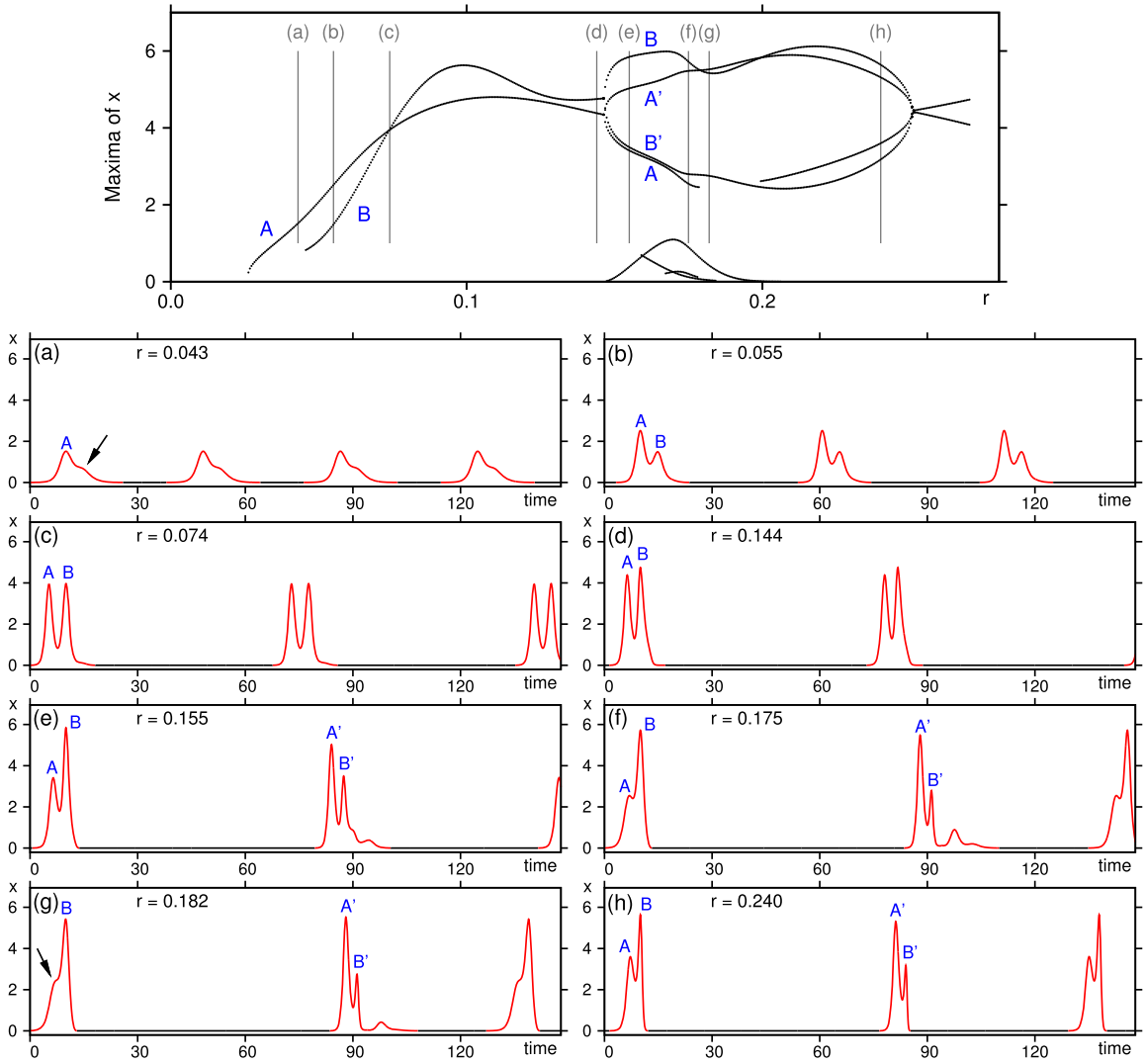

Fig. 2. Top panel: bifurcation diagram for $0 < r < 0.27$, $B = 0.25$, and $\tau = 3$ μs (as indicated by the black line in the corresponding panel in Fig. 1). Bottom panel (a)–(h): temporal evolution for values of r indicated by the vertical lines in the bifurcation diagram. Black horizontal segments indicate laser off (i.e., $x < 0.005$).

temporal evolutions inside these islands become more complex as τ evolves. To clarify how the laser output is altered and generates such structures, we draw a bifurcation diagram, shown on the top row of Fig. 2, for parameters values cutting the concentric islands located inside the green region (2 peaks) in the panel for $\tau = 3.0$ μs, in Fig. 1. This bifurcation diagram is calculated along the horizontal black line of this panel, crossing over the structure in question, and clearly presents a combination of the well-known peak-doubling bifurcation and the abrupt appearance and disappearance of isolated branches, resulting from the peak generation by continuous deformation of the temporal solution as the parameter is varied (the "peak-adding phenomenon" [7,41]).

Figures 2(a)–2(h) show the temporal evolution of the laser intensity x (in arbitrary units) for representative values of r, indicated by vertical lines in the bifurcation diagram. Figure 2(a) shows the peak A corresponding to the branch A on the bifurcation diagram. In this figure, the arrow indicates a deformation in the laser pulse that, upon further increase of r, gives origin to a new peak B, associated with the branch B and is clearly visible in Fig. 2(b). Initially, the amplitude of peak B is smaller than A, but as r increases, its amplitude grows faster, with B eventually becoming larger than A. This unfolding can be followed in Figs. 2(b)–2(d). As r further increases past a bifurcation, which occurs for $r \approx 0.146$, peaks A and B split into doublets (A, A′) and (B, B′), as shown in Fig. 2(e). This happens such that peak A′, born smaller than B, grows faster than B, overtaking it at $r = 0.179$ and remaining so until $r = 0.199$, when peak B becomes bigger again. Curiously, in the range of r where A′ remains bigger than B, the peak A disappears, returning when B becomes bigger than A′ again. This phenomenon may be seen in Figs. 2(f)–2(h) and following the evolution of branches B, A′, and A in the bifurcation diagram. Peak A disappears smaller but reappears larger than B′.

The top panel in Fig. 2 contains nonlabeled small peaks visible at the bottom of the bifurcation diagram, immediately after peak B′ in Figs. 2(e)–2(g). Such peaks are born and disappear obeying the same peak-adding mechanism described above. The difference is that, in those regions, the continuous deformations are changing the solution on a smaller scale.

5. SPIKING ON $\tau \times R$ AND $\tau \times B$ DIAGRAMS

In this section, we consider the modal structure in two additional control planes, $\tau \times r$ and $\tau \times B$. The motivation is to learn what sort of changes the modes undergo as a function of the feedback gain r and the bias voltage B applied to the electro-optic modulator as a function of the delay τ.

Figure 3(a) shows an extended portion of the $\tau \times r$ plane, computed for $B = 0.25$, the same value used in Fig. 1. This

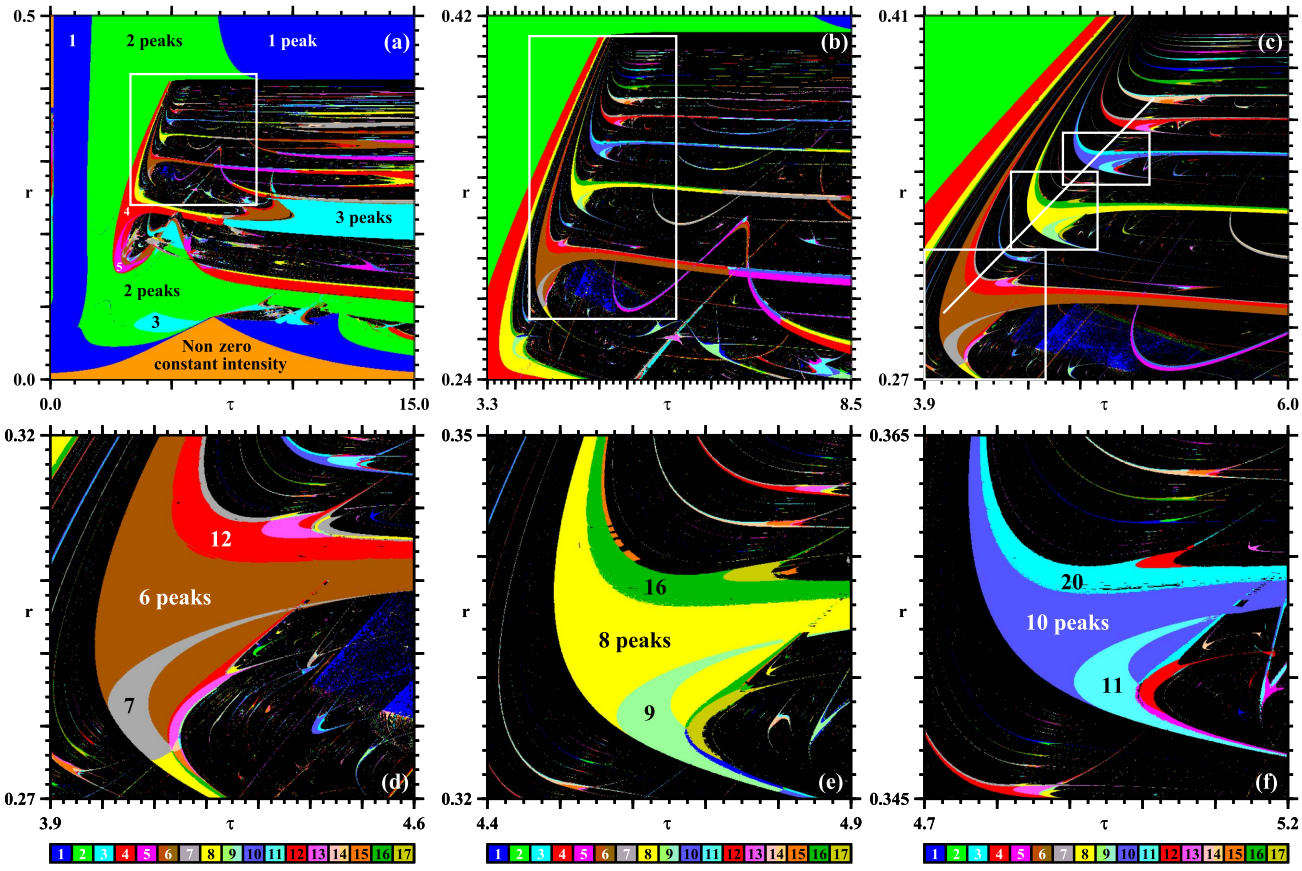

Fig. 3. Top row: parameter windows illustrating the complex accumulation of stable laser phases on the $\tau \times r$ for $B = 0.25$. Along the line segment in (c), the number of spikes of the laser pulses increase by two as r increases, accumulating on the large window characterized by pulsations with two spikes. In (c), one also recognizes that self-pulsations have a constant number of spikes along the horizontal stripes forming shrimp [45–47] legs. The bottom row shows that peak doubling and adding occurs *simultaneously* inside the shrimps. Each panel shows 600 × 600 parameter points.

diagram reveals a number of remarkable facts about the peculiar self-organization of the laser pulsations. For $r \lesssim 0.15$, one essentially finds solutions having either a nonzero constant amplitude or simple periodic oscillations with one peak per period. For r small enough, the laser does not oscillate independently of the value of the delay. In other words, the dimensionality jump of the phase space plays no role in sufficiently small delays. Complex oscillatory modes become possible above $r \simeq 0.15$, first in small domains for relatively large values of τ of the order of $\tau \gtrsim 7$ μs.

A conspicuous feature observed in Fig. 3(a) as r grows is the large green phase, which denotes oscillations with two peaks per period. This phase dominates the left side of the stability diagram, together with the black domain representing nonperiodic, "chaotic," laser modes. Oscillations with a larger number of spikes per period become also abundant for $r \gtrsim 1.5$ and $\tau \gtrsim 3$ μs. As indicated in the figure, when r grows in that region, one sees what in this scale appears to be an abrupt transition from 2 to 5 pulses per period. Under magnification, it is possible to realize the existence of a $2 \rightarrow 4$ peak-doubling and then a $4 \rightarrow 5$ adding. The right-hand-side boundary of the 2-peaks green phase displays a peak-doubling cascade, seen more clearly in Fig. 3(b). Following this doubling cascade there is an alignment of shrimps [45–47], namely a sequence of self-similar periodic phases with complex internal distribution of modes, with number of peaks that grow apparently without bound. Such sequence is shown magnified in Fig. 3(c), where a line segment indicates the direction along which the phases accumulate as r grows. To move along this line requires tuning two parameters simultaneously.

The three shrimps inside white boxes Fig. 3(c) are magnified in the bottom row of the figure. Each panel displays the number of peaks for the three largest of the infinite number of phases belonging to the shrimps in Figs. 3(d)–3(f): (6,12,7), (8,16,9), and (10,20,11), respectively. In such shrimps, the number of peaks of the largest stability region grows by two from shrimp to shrimp when r grows toward the green accumulation boundary of two peaked oscillations. The next two largest regions reveal a surprising mode unfolding: while in the upper region laser oscillations follow a *peak-doubling* cascade, in the lower region they follow a *peak-adding* cascade [7,41]. More complex mode subdivisions are clearly visible, but they are more difficult to characterize systematically by other means than graphically.

Figure 4 shows results similar to Fig. 3 but for the $\tau \times B$ control plane. *Mutatis mutandis* laser modes organize quite similarly in both planes. In particular, cascades of peak doublings and addings as well as their accumulations can be followed with no difficulty by suitably tuning parameters from top to bottom along the white line in Fig. 4(d).

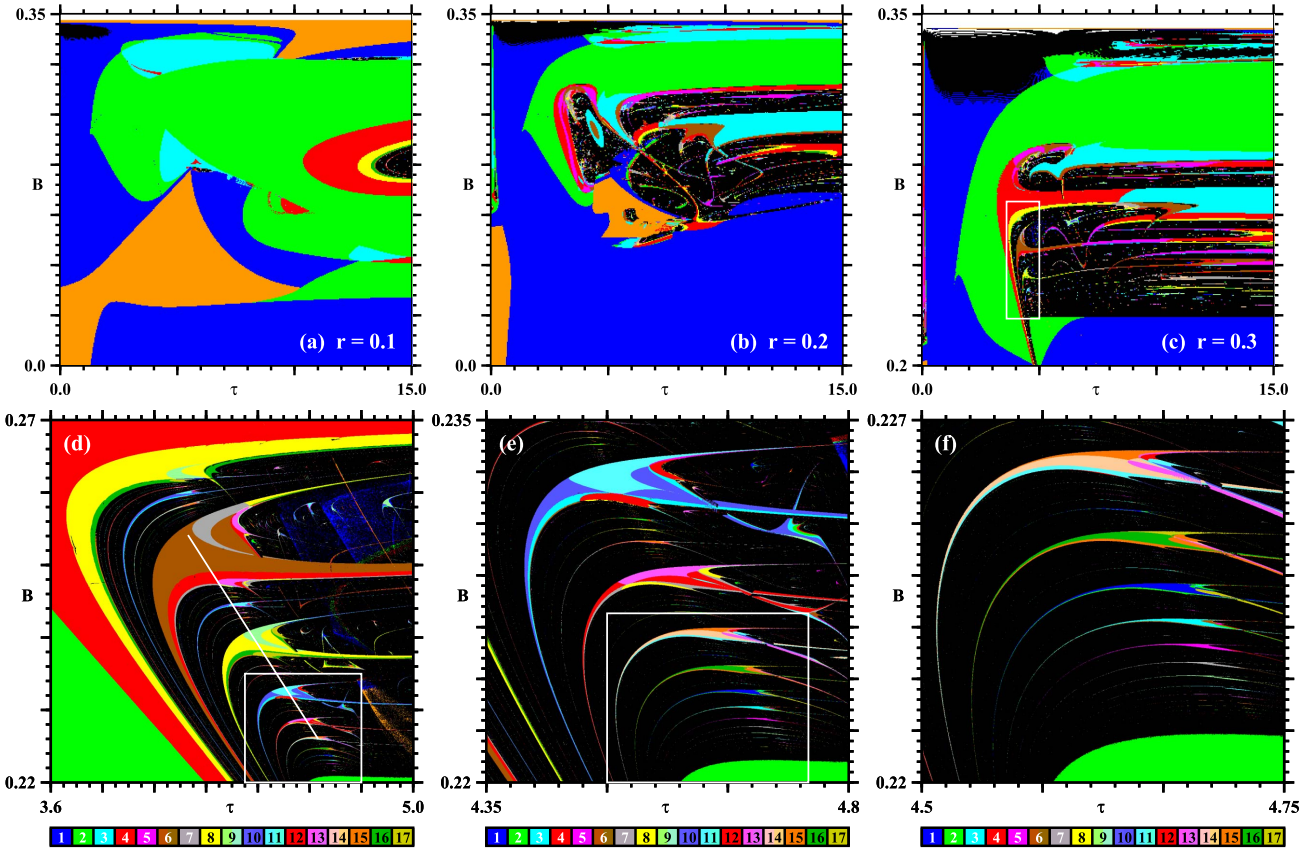

Fig. 4. Top row: global views of control plane $\tau \times B$ for different values of r. The box in (c) is magnified in panel (d). Bottom row: successive magnifications of the box (c), illustrating a typical downward accumulation cascade of periodic laser modes. In (d), the line segment runs from (4.130, 0.25413) to (4.633, 0.22599). As in Fig. 3, from shrimp to shrimp the number of peaks of the largest phase increases by two peaks via a doublet-adding mechanism (see text). Each panel shows 1200×1200 parameter points.

Figure 5 presents additional information concerning the unfolding of oscillatory modes along the white lines in Figs. 3(c) and 4(d). The idea of this figure is to further clarify details of the nature and organization of laser pulsations. In Fig. 5, the top panels are bifurcation diagrams depicting local maxima of the laser intensity x recorded along the pair of white lines, defined by the equations

$$r = -0.005705 + 0.073480\tau, \qquad \tau \in [4.0992, 5.2287], \quad \textbf{(4)}$$

$$B = 0.485214 - 0.055952\tau, \qquad \tau \in [4.1300, 4.6330]. \quad \textbf{(5)}$$

Note that, to be able to follow such accumulation cascades, one must tune two parameters simultaneously. Both bifurcation diagrams look quite similar, their ordering as well as the cascade unfolding inside every periodicity window, configuring a surprising isomorphism and signaling to symmetries in the underlying surface embedded in the multidimensional space formed by all control parameters.

Figures 3(d)–3(f) manifested clearly the self-similar shrimp nature. In contrast with the more common structure [45], inside them one now finds combined cascades of peak-doubling and peak adding. In addition, Figs. 3 and 4 revealed that, in such cascades, the number of peaks of the phases with largest "volume" increases by two units from shrimp to shrimp. In this context, a natural question to ask is what sort of changes laser modes undergo when proceeding along the cascades. The answer is given in Fig. 5 for both cascades. The left column refers to the march along Eq. (4), for Fig. 3, while the right column refers to Eq. (5), for Fig. 4. The top panels in Fig. 5 show bifurcation diagrams for intervals defined in Eqs. (4)

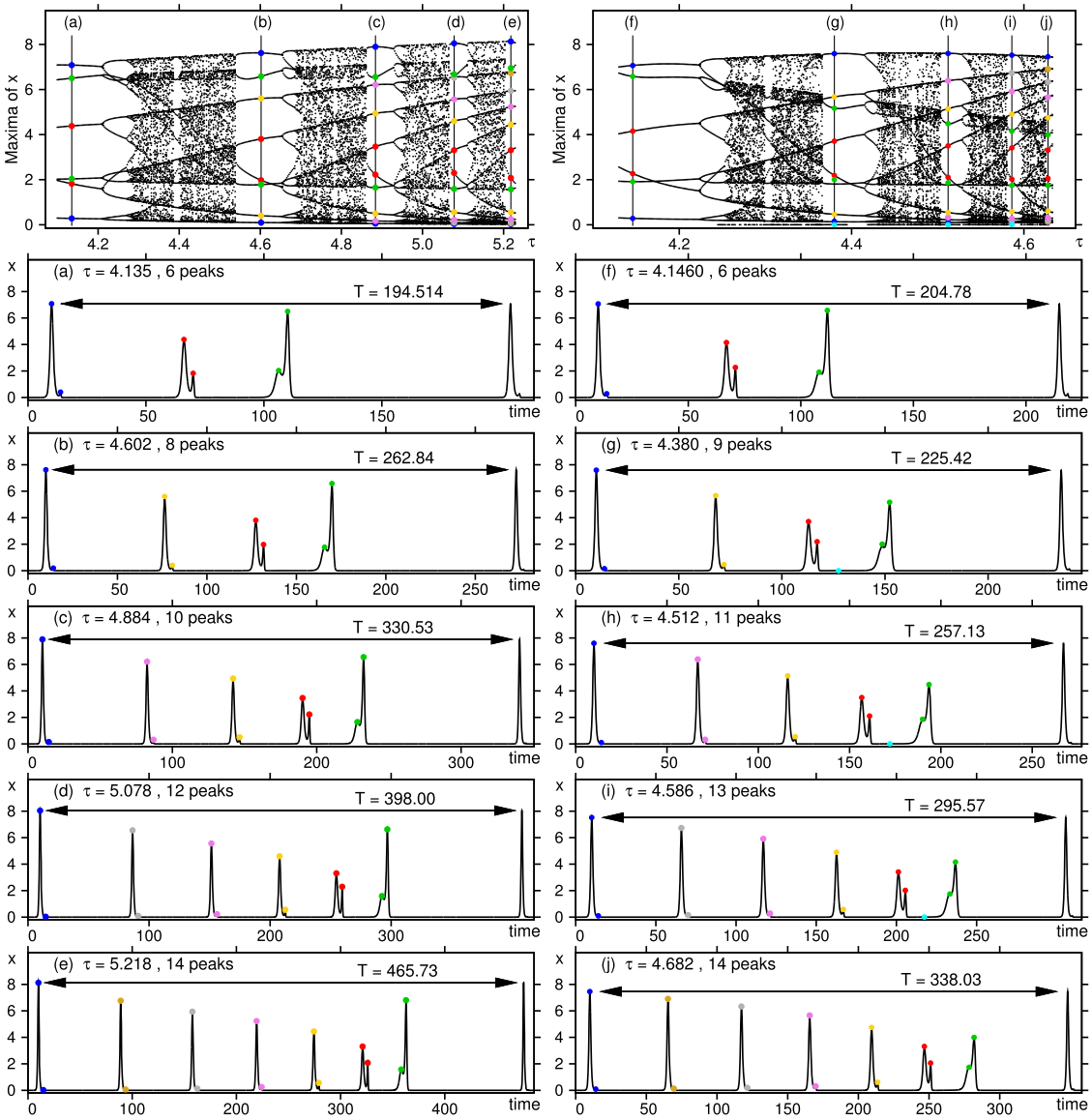

Fig. 5. Top-left: bifurcation diagram calculated for Eq. (4), namely, over the white line (crossing the shrimps) in the $\tau \times r$ diagram of Fig. 3(c). (a)–(e): Temporal evolution showing laser oscillations near the "center" of the shrimps, marked by vertical lines in the bifurcation diagram. Top-right: bifurcation diagram calculated for Eq. (5), namely, over the white line in the $\tau \times B$ diagram of Fig. 4(d). (f)–(j): Corresponding temporal evolutions at the vertical lines in the bifurcation diagram.

and (5). They contain five vertical lines labeled from (a) to (e), on the left panel, and from (f) to (j), on the right. Parameters defined by these vertical lines are located at the center of the shrimps discussed above. The temporal evolution for the selected parameters is displayed on the panels below the bifurcation diagrams.

Figures 5(a)–5(e) show the temporal evolution along the cascade on the $\tau \times r$ control plane. Figure 5(a) refers to the first shrimp, where the oscillation shows six peaks per period. This pattern is periodic, formed by the repetition of three pulse doublets, indicated by blue, red, and green dots, each doublet consisting of a small and a big pulse. Similar colored dots are also used to identify the branches that the pulses produce in the bifurcation diagram. The oscillations of the next shrimp, Fig. 5(b), have eight peaks per period: the same three doublets as before plus a new doublet marked with yellow dots. Next, Fig. 5(c) shows 10 peaks per period: the four previous doublets plus a new doublet, marked in violet. This peak-doublet addition persists in subsequent shrimps, a new doublet being added to the large peak on the left when one moves from shrimp to shrimp, as illustrate for two more steps in Figs. 5(d) and 5(e). This doublet-adding mechanism mimics a similar mechanism observed previously by us in a considerable simpler scenario, involving a single delay-differential equation describing a physiological delayed system, the prototypical Mackey and Glass system associated with *dynamical diseases* [41].

Figures 5(a)–5(e) also record the period T of the oscillations, revealing a roughly constant period increment from shrimp to shrimp: $262.84 - 194.514 = 68.326$, $330.53 - 262.84 = 67.69$, $398.0 - 330.53 = 67.47$, $465.73 - 398.0 = 67.73$. Figures 5(f)–5(j) show that the doublet-adding mechanism is also at work on the $\tau \times B$ control plane. First, note that, in Fig. 4(d), the white line misses the parabolic 7-peaks arc. This shows that generic accumulations occur along slightly curved paths, which, however, are well approximated by line segments. The mild curvature explains why the doublet-adding mechanism starts from Fig. 5(g) [not from Fig. 5(f)]. More specifically, the difference between the two sequences of temporal evolutions in Fig. 5 is that a new and very small peak appears in Figs. 5(g)–5(j), indicated by a light blue dot, due to the fact that, differently from the white line in Fig. 3(c), the white line in Fig. 4(d) now crosses the corresponding shrimps over the region of peak-adding, near the top of such structures. Apart from the curvature deviation, the unfolding in both columns is the same. On the right columns, the increments of the periods are $257.13 - 225.42 = 31.71$, $295.57 - 257.13 = 38.44$, $338.03 - 295.57 = 42.46$. Now, the period is also increasing but the increments get bigger from shrimp to shrimp. This marked difference should not be difficult to observe in experiments.

6. CONCLUSIONS AND OUTLOOK

Thus far, stability charts for CO_2 lasers with feedback were known only for the $r \times B$ control plane and for instantaneous feedback ($\tau = 0$ μs). Such results have now been considerably extended, revealing what happens in the presence of delayed feedbacks of arbitrary duration τ. Broadly speaking, we described the existence of three delay regimes for the $r \times B$ control space. As described in Section 3, these laser stability delays for each of these regimes differ from the current expectations for delayed lasers.

Laser phases display several hitherto unseen features such as, for example, a series of shrimp accumulations associated with the emergence of concentric islands of periodic oscillations in control space, with increasing complexity (greater number of peaks per period) combining sequences of peak-doubling and peak-adding cascades, resembling in some aspects what was observed recently in the flow governing a complex enzyme reaction [43,53]. The effect of the emerging islands on the temporal profile of the laser intensity has been elucidated. To observe such remarkable variations in laser pulsations, one must adjust two parameters simultaneously.

We also reported stability charts for two additional control planes of the laser, namely, the $\tau \times r$ and $\tau \times B$ planes shown in Figs. 3 and 4, respectively. Modal distribution in these distinct planes looks surprisingly similar, isomorphic. The characteristic signature of the mode complexification along such cascades was found to consist of a doublet-adding mechanism, which can come in two varieties: either displaying a constant or nonconstant increase of the period of the largest phase of adjacent shrimps. In experiments, the simultaneous variation of two parameters started to be considered in high resolution only quite recently—not for lasers but in experiments involving electronic circuits [54]. In this respect, the detailed diagrams presented here can contribute to finding suitable configurations to conduct laser experiments. Lasers are well-known systems for traditionally revealing a plethora of fundamental and applied novelties. We hope that the simulations reported here may help to motive their experimental corroboration in the near future.

Funding. CNPq/Brazil; Deutsche Forschungsgemeinschaft.

Acknowledgment. The authors were supported by CNPq/Brazil. All bitmaps were computed on the CESUP-UFRGS clusters, located in Porto Alegre, Brazil. This work was also supported by the Deutsche Forschungsgemeinschaft through the Cluster of Excellence *Engineering of Advanced Materials*.

REFERENCES

1. N. Jiang, W. Pan, L. Yan, B. Luo, S. Xiang, L. Yang, and D. Zheng, "Isochronal chaos synchronization of semiconductor lasers with multiple time-delayed couplings," J. Opt. Soc. Am. B **28**, 1139–1145 (2011).
2. M. Sciamanna, A. Tabaka, H. Thienpont, and K. Panajotov, "Intensity behavior underlying pulse packages in semiconductor lasers that are subject to optical feedback," J. Opt. Soc. Am. B **22**, 777–785 (2005).
3. M. Sciamanna, C. Masoller, N. Abraham, F. Rogister, P. Mégret, and M. Blondel, "Different regimes of low-frequency fluctuations in vertical-cavity surface-emitting lasers," J. Opt. Soc. Am. B **20**, 37–44 (2003).
4. E. J. Doedel and C. L. Pando, "Multiparameter bifurcations and mixed-mode oscillations in Q-switched CO_2 lasers," Phys. Rev. E **89**, 052904 (2014).
5. E. J. Doedel and C. L. Pando, "Isolas of periodic passive Q-switching self-pulsations in the three-level: two-level model for a laser with a saturable absorber," Phys. Rev. E **84**, 056207 (2011).
6. E. J. Doedel, B. E. Oldeman, and C. L. Pando, "Bifurcation structures in a model of a CO_2 laser with a fast saturable absorber," Int. J. Bifurcation Chaos Appl. Sci. Eng. **21**, 305–322 (2011).

7. L. Junges and J. A. C. Gallas, "Frequency and peak discontinuities in self-pulsations of a CO_2 laser with feedback," Opt. Commun. **285**, 4500–4506 (2012).
8. W. Vandermeiren, J. Stiens, G. Shkerdin, and R. Vounckx, "Theoretical analysis of partial-spatial *Q*-switching dynamics using a two-level CO_2 laser model," IEEE J. Quantum Electron. **48**, 447–453 (2012).
9. J. G. Freire, R. Meucci, F. T. Arecchi, and J. A. C. Gallas, "Self-organization of pulsing and bursting in a CO_2 laser with opto-electronic feedback," Chaos **25**, 097607 (2015).
10. T. Erneux and P. Glorieux, *Laser Dynamics* (Cambridge University, 2010).
11. F. T. Arecchi, W. Gadomski, and R. Meucci, "Generation of chaotic dynamics by feedback on a laser," Phys. Rev. A **34**, 1617–1620 (1986).
12. J. R. Tredicce, F. T. Arecchi, G. P. Puccioni, A. Poggi, and W. Gadomski, "Dynamic behavior and onset of low-dimensional chaos in a modulated homogeneously broadened single-node laser: experiments and theory," Phys. Rev. A **34**, 2073–2081 (1986).
13. F. T. Arecchi, *Instabilities and Chaos in Quantum Optics* (Springer, 1987).
14. F. T. Arecchi, R. Meucci, and W. Gadomski, "Laser dynamics with competing instabilities," Phys. Rev. Lett. **58**, 2205–2208 (1987).
15. F. T. Arecchi, W. Gadomski, A. Lapucci, H. Mancini, R. Meucci, and J. A. Roversi, "Laser with feedback: an optical implementation of competing instabilities, Shilnikov chaos, and transient fluctuation enhancement," J. Opt. Soc. Am. B **5**, 1153–1159 (1988).
16. F. T. Arecchi, A. Lapucci, R. Meucci, J. A. Roversi, and P. H. Coullet, "Experimental characterization of Shilnikov chaos by statistics of return times," Europhys. Lett. **6**, 677–682 (1988).
17. F. T. Arecchi, W. Gadomski, R. Meucci, and J. A. Roversi, "Delayed bifurcation at the threshold of a swept gain CO_2 laser," Opt. Commun. **70**, 155–160 (1989).
18. P. Y. Wang, A. Lapucci, R. Meucci, and F. T. Arecchi, "Onset of subcritical bifurcation in a CO_2 laser with feedback," Opt. Commun. **80**, 42–46 (1990).
19. R. Meucci, A. Labate, and M. Ciofini, "Controlling chaos by negative feedback of subharmonic components," Phys. Rev. E **56**, 2829–2834 (1997).
20. A. N. Pisarchik, R. Meucci, and F. T. Arecchi, "Theoretical and experimental study of discrete behavior of Shilnikov chaos in a CO_2 laser," Eur. Phys. J. D **13**, 385–391 (2001).
21. Q. S. Yang, P. Y. Wang, H. W. Yin, J. H. Dai, and H. J. Zhang, "Global stability and oscillation properties of a two-level model for a class B laser with feedback," Opt. Commun. **138**, 325–329 (1997).
22. J. Ohtsubo, *Semiconductor Lasers: Stability, Instability and Chaos* (Springer, 2013).
23. D. M. Kane and K. A. Shore, *Unlocking Dynamical Diversity: Optical Feedback Effects on Semiconductor Lasers* (Wiley, 2005).
24. S. Strogatz, *Nonlinear Dynamics and Chaos with Applications to Physics, Biology, Chemistry, and Engineering* (Westview, 2015).
25. F. T. Arecchi, R. Meucci, G. Puccioni, and J. Tredicce, "Experimental evidence of subharmonic bifurcations, multistability, and turbulence in a Q-switched gas laser," Phys. Rev. Lett. **49**, 1217–1220 (1982).
26. C. Bonatto, J. C. Garreau, and J. A. C. Gallas, "Self-similarities in the frequency-amplitude space of a loss-modulated CO_2 laser," Phys. Rev. Lett. **95**, 143905 (2005).
27. C. Bonatto and J. A. C. Gallas, "Accumulation boundaries: codimension-two accumulation of accumulations in phase diagrams of semiconductor lasers, electric circuits, atmospheric, and chemical oscillators," Philos. Trans. R. Soc. London Ser. A **366**, 505–517 (2008).
28. F. T. Arecchi, G. L. Lippi, G. P. Puccioni, and J. R. Tredicce, "Deterministic chaos in laser with injected signal," Opt. Commun. **51**, 308–314 (1984).
29. J. Argyris, G. Faust, M. Haase, and R. Friedrich, *An Exploration of Dynamical Systems and Chaos* (Springer, 2015).
30. C. Otto, K. Lüdge, A. G. Vladimirov, M. Wolfrum, and E. Schöll, "Delay-induced dynamics and jitter reduction of passively mode-locked semiconductor lasers subject to optical feedback," New J. Phys. **14**, 113033 (2012).
31. B. Lingnau, W. W. Chow, E. Schöll, and K. Lüdge, "Feedback and injection locking instabilities in quantum-dot lasers: a microscopically based bifurcation analysis," New J. Phys. **15**, 093031 (2013).
32. E. Schöll and H. G. Schuster, *Handbook of Chaos Control* (Wiley, 2007).
33. M. Sciamanna and K. A. Shore, "Physics and applications of laser diode chaos," Nat. Photonics **9**, 151–162 (2015).
34. F. T. Arecchi, G. Giacomelli, A. Lapucci, and R. Meucci, "Dynamics of a CO_2 laser with delayed feedback: the short-delay regime," Phys. Rev. A **43**, 4997–5004 (1991).
35. L. Junges and J. A. C. Gallas, "Stability diagrams for continuous wide-range control of two mutually delay-coupled semiconductor lasers," New J. Phys. **17**, 053038 (2015).
36. M. Lakshmanan and D. V. Senthilkumar, *Dynamics of Nonlinear Time-Delay Systems* (Springer, 2010).
37. J. G. Freire and J. A. C. Gallas, "Stern–Brocot trees in the periodicity of mixed-mode oscillations," Phys. Chem. Chem. Phys. **13**, 12191–12198 (2011).
38. J. G. Freire and J. A. C. Gallas, "Stern-Brocot trees in cascades of mixed-mode oscillations and canards in the extended Bonhoeffer-van der Pol and the FitzHugh-Nagumo models of excitable systems," Phys. Lett. A **375**, 1097–1103 (2011).
39. M. A. Nascimento, J. A. C. Gallas, and H. Varela, "Self-organized distribution of periodicity and chaos in an electrochemical oscillator," Phys. Chem. Chem. Phys. **13**, 441–446 (2011).
40. J. G. Freire, R. J. Field, and J. A. C. Gallas, "Relative abundance and structure of chaotic behavior: The nonpolynomial Belousov-Zhabotinsky reaction kinetics," J. Chem. Phys. **131**, 044105 (2009).
41. L. Junges and J. A. C. Gallas, "Intricate routes to chaos in the Mackey-Glass delayed feedback system," Phys. Lett. A **376**, 2109–2116 (2012).
42. L. Junges, T. Pöschel, and J. A. C. Gallas, "Characterization of the stability of semiconductor lasers with delayed feedback according to the Lang-Kobayashi model," Eur. Phys. J. D **67**, 149 (2013).
43. M. R. Gallas and J. A. C. Gallas, "Nested arithmetic progressions of oscillatory phases in Olsen's enzyme reaction model," Chaos **25**, 064603 (2015).
44. R. Meucci, S. Euzzor, E. Pugliese, S. Zambrano, M. R. Gallas, and J. A. C. Gallas, "Optimal phase-control strategy for damped-driven Duffing oscillators," Phys. Rev. Lett. **116**, 044101 (2016).
45. J. A. C. Gallas, "Structure of the parameter space of the Hénon map," Phys. Rev. Lett. **70**, 2714–2717 (1993).
46. E. N. Lorenz, "Compound windows of the Hénon-map," Physica D **237**, 1689–1704 (2008).
47. W. Façanha, B. Oldeman, and L. Glass, "Bifurcation structures in two-dimensional maps: the endoskeletons of shrimps," Phys. Lett. A **377**, 1264–1268 (2013).
48. M. C. Soriano, J. Garcia-Ojalvo, C. R. Mirasso, and I. Fisher, "Complex photonics: dynamics and applications of delay-coupled semiconductors lasers," Rev. Mod. Phys. **85**, 421–470 (2013).
49. S. Yanchuk and P. Perlikowski, "Delay and periodicity," Phys. Rev. E **79**, 046221 (2009).
50. S. Yanchuk and M. Wolfrum, "A multiple time scale approach to the stability of external cavity modes in the Lang-Kobayashi system using the limit of large delay," SIAM J. Appl. Dyn. Sys. **9**, 519–535 (2010).
51. M. Wolfrum, S. Yanchuk, P. Hövel, and E. Schöll, "Complex dynamics in delay-differential equations with large delay," Eur. Phys. J. Spec. Top. **191**, 91–103 (2010).
52. V. Kovanis, A. Gavrielides, and J. A. C. Gallas, "Labyrinth bifurcations in optically injected diode lasers," Eur. Phys. J. D **58**, 181–186 (2010).
53. M. J. B. Hauser and J. A. C. Gallas, "Nonchaos-mediated mixed-mode oscillations in an enzyme reaction system," J. Phys. Chem. Lett. **5**, 4187–4193 (2014).
54. A. Sack, J. G. Freire, E. Lindberg, T. Pöschel, and J. A. C. Gallas, "Discontinuous spirals of stable periodic oscillations," Sci. Rep. **3**, 3350 (2013).